Lanthanides

DOI: 10.1002/anie.201208218

Breakdown of Crystallographic Site Symmetry in Lanthanide-Doped $NaYF_4$ Crystals**

*Datao Tu, Yongsheng Liu, Haomiao Zhu, Renfu Li, Liqin Liu, and Xueyuan Chen**

Trivalent lanthanide ions (Ln^{3+}) are well-known for their luminescent properties and have been utilized for decades in television sets and fluorescent lights. More recently, Ln^{3+}-doped inorganic nanoparticles, emerging as a new class of bioprobes, have attracted revived interest for their promising applications in bioimaging and biosensing owing to their superior features such as intense, long-lived, and multicolor emissions.[1] The optical transitions of Ln^{3+} are sensitive to their local coordination, and the emission intensity of Ln^{3+}-based compounds strongly depends on the crystal structure and crystal-field (CF) surroundings around Ln^{3+}.[2] Therefore, Ln^{3+} ions are often used as probe to analyze the local structure of cations in luminescent materials.[3] However, for one family of inorganic crystals with disordered structures, such as molybdates and tungstates in which two or more cations statistically occupy the same lattice site, the symmetry of spectroscopic sites for the dopant Ln^{3+} ions was observed to deviate from that of crystallographic sites.[4] Because the microscopic model of such structural disorder is established from a least-squares fitting of single-crystal X-ray diffraction (XRD) data by standard crystallography analysis, which takes into account those cations randomly occupying the same lattice site as a virtual "average" ion with their respective probabilities, the actual local symmetry of the dopant in the disorder site can not be revealed from the crystallographic data.[5] To date, only one report has attempted to resolve the apparent symmetry distortion between the crystallographic sites and spectroscopic sites by diffuse X-ray scattering.[5] Unfortunately, the mechanism behind this breakdown of crystallographic site symmetry in an average structure remains essentially untouched. Nowadays, disordered crystals with distinct optical properties are widely used as host materials for lighting and displays, lasers, or bioassays. An unambiguous spectroscopic revelation of local site symmetry breakdown in this huge family of crystals is crucial to optimizing their optical performance for further applications.

Among various host materials with disordered structures, inorganic fluorides $AREF_4$ (A = alkali metal, RE = rare-earth metal), are excellent hosts for Ln^{3+} doping owing to their low phonon frequencies and high chemical stability.[6] Although Yb^{3+}/Er^{3+} (or Yb^{3+}/Tm^{3+}) co-doped cubic (α) or hexagonal (β) phase $NaYF_4$ phosphors are regarded as the most efficient near-infrared-to-visible upconversion (UC) materials,[7] the spectroscopic or crystallographic site of Ln^{3+} in $NaYF_4$, particularly in β-$NaYF_4$, has received much debate, and two different symmetries have been proposed from previous optical studies.[5,8] The structure of β-$NaLnF_4$ was first investigated in 1965; β-$NaNdF_4$ has the space group $P\bar{6}$ with two kinds of Nd^{3+} sites in the lattice, while β-$NaYF_4$ has $P6_3/m$, and contains only one kind of Y^{3+} with a crystallographic site symmetry of C_{3h}.[8a] Since then, this pioneering work has been extensively cited for the description of the β-$NaYF_4$ structure, among which quite a few researchers confused the structure of β-$NaNdF_4$ with β-$NaYF_4$ they synthesized and unintentionally regarded $P\bar{6}$ as the space group of β-$NaYF_4$.[5,9] On the other hand, it has been argued that the space group for β-$NaYF_4$ was $P\bar{6}$ at near ambient pressures and $P6_3/m$ only at high pressures above 20 GPa through high-pressure crystal structure analysis in 2002.[10] However, according to the structural parameters of $P\bar{6}$ for β-$NaYF_4$, the derived mean bond length of Y1-F, which was anomalously larger than that of Y2/Na-F, thus remains suspicious from the crystallographic point of view. The space group was recently confirmed as $P6_3/m$ and only one Y site (C_{3h}) is partially occupied by Na in non-stoichiometric β-$NaYF_4$ powders.[8b] As Eu^{3+} ions are usually employed as an excellent optical probe to decipher the coordination environment around the substituted cations in the crystalline lattice,[3a] we anticipate that the above controversy over the local site symmetry of emitters in $NaYF_4$ can be resolved from the high-resolution spectra of doped Eu^{3+} ions.

Both α- and β-$NaYF_4$ are disordered crystals in which Na^+ and Y^{3+} ions are randomly distributed over the same lattice site.[1g] Once the probe ions (Eu^{3+}) are doped into such disordered crystals to substitute for Y^{3+}, the coordination environment around the dopant will unavoidably be changed because of the mismatch of ionic radius between Eu^{3+} (0.95 Å) and Y^{3+} (0.89 Å).[3a] As a result, the real symmetry of spectroscopic sites of Eu^{3+} may differ drastically from that of crystallographic sites of Y^{3+}. Previous reports on the low-temperature spectra of β-$NaYF_4$:Eu^{3+} observed the possible multiple Eu^{3+} sites based on the presence of more transitions of Eu^{3+} than theoretically expected.[11] However, these formerly investigated samples generally suffered from impur-

[*] Dr. D. T. Tu, Dr. Y. S. Liu, Dr. H. M. Zhu, R. F. Li, Dr. L. Q. Liu, Prof. Dr. X. Y. Chen
Key Laboratory of Optoelectronic Materials Chemistry and Physics, Fujian Institute of Research on the Structure of Matter, Chinese Academy of Sciences
Fuzhou, Fujian 350002 (China)
E-mail: xchen@fjirsm.ac.cn

[**] We thank Prof. Ning Ye for helpful discussion about the crystallographic site symmetry in α- and β-$NaYF_4$. This work is supported by the NSFC (Nos. 10974200, 11204302, 51102234, and 51002151), the 863 program of MOST (No. 2011AA03A407), and the NSF of Fujian Province for Young Scientists (Nos. 2010J05126, 2011J05145, and 2012J05106).

Supporting information for this article is available on the WWW under http://dx.doi.org/10.1002/anie.201208218.

ities of cubic $NaYF_4$ or YOF.[8b] No effort has been made to perform the CF analysis and thus to reveal the crystallographic site symmetry breaking of Eu^{3+} in $NaYF_4$ phosphors. The origin of symmetry distortion between the crystallographic and spectroscopic sites in disordered hosts remains a challenge.

Herein, the local structure and site symmetry of Eu^{3+} in disordered $NaYF_4$ crystals are investigated in detail based on high-resolution excitation and emission spectra at low temperature. The CF parameters of Eu^{3+} in both α- and β-$NaYF_4$ phosphors are determined for the first time to verify the local site symmetry breakdown from crystallographic O_h or C_{3h}. Furthermore, such a breakdown of crystallographic site symmetry is also found in other Ln^{3+}-doped disordered crystals, such as $KGdF_4$ and KYF_4.

High-quality α- and β-$NaYF_4$:Eu^{3+} crystals were synthesized by a facile hydrothermal method.[6b,c] SEM images show that the as-prepared α-$NaYF_4$:Eu^{3+} samples are spherical particles with a diameter of about 350 nm, and the β-$NaYF_4$:Eu^{3+} samples are submicrometer rods with an average size of 300 nm in diameter and 700 nm in length (Supporting Information, Figure S1). As the chemical valence of Eu^{3+} is the same as that of Y^{3+}, and the ionic radius of Eu^{3+} is close to that of Y^{3+},[3a] Eu^{3+} can be easily doped into the Y lattice of $NaYF_4$. Composition analyses by the energy dispersive X-ray (EDX) spectrum confirm the presence of Na, Y, F, and doped Eu elements in both α- and β-$NaYF_4$ phosphors (Supporting Information, Figure S1). The XRD peaks of α-$NaYF_4$:Eu^{3+} can be assigned to pure cubic $NaYF_4$ (JCPDS No. 77-2042, $Fm\bar{3}m$), while all the diffraction peaks of β-$NaYF_4$:Eu^{3+} can be indexed to hexagonal $NaYF_4$ without any other impurity phases (Supporting Information, Figure S2). The space group of hexagonal $NaYF_4$ was controversially given as either $P6_3/m$ or $P\bar{6}$, which can not be easily distinguished from the XRD data owing to the tiny difference in their patterns (namely, presence of very weak intensity for the (001) reflection at $2\theta = 25.4°$ for $P\bar{6}$).[5,9d]

Figure 1 illustrates the doping-induced breakdown of crystallographic site symmetry for Eu^{3+} in α- and β-$NaYF_4$ crystals (the positional parameters of α-$NaYF_4$ and β-$NaYF_4$ with space groups of $Fm\bar{3}m$ and $P6_3/m$ (or $P\bar{6}$) are listed in the Supporting Information, Table S1). The average structure of α-$NaYF_4$ from single-crystal XRD data is a derivative CaF_2 fluorite type with the Ca^{2+} site (4a) randomly occupied by 1/2 Na^+ and 1/2 Y^{3+}: the nearest-neighboring ions around Y^{3+} on site 4a are 8 F^-, and the second-nearest-neighboring ions are 6 Na^+ and 6 Y^{3+}.[1g] The crystallographic symmetry for Y^{3+} ions on site 4a is O_h (Figure 1a). When Eu^{3+} ions are doped in the Y lattice of α-$NaYF_4$, in view of the larger ionic radius of Eu^{3+} relative to that of Y^{3+}, the bond length of Eu-F is supposed to be longer than that of Y-F, which thus perturbs the coordination shell around site 4a originally statistically distributed by Y^{3+} and Na^+. Accordingly, the displacement patterns of various Y/Na combinations in the second coordination shell around each subset of Eu could be slightly different. Based on the microscopic model of disorder,[5] the local site symmetry of each subset of Eu^{3+} will be reduced from O_h to lower symmetry, such as C_s, C_2, or even C_1. Particularly, if the second coordination shell with Y/Na on site 4a around one subset of

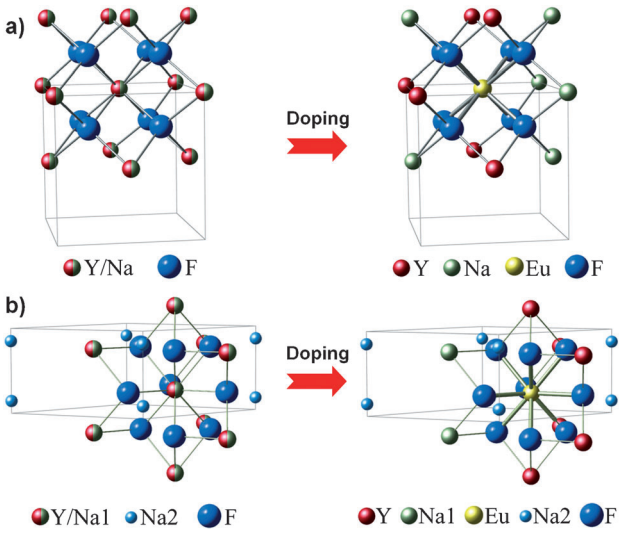

Figure 1. Illustration showing the breakdown of crystallographic site symmetry of Eu^{3+} in a) α-$NaYF_4$ and b) β-$NaYF_4$ crystals. Induced by Ln^{3+}-doping for the disordered Y/Na site, the original crystallographic site symmetries of O_h in (a) and C_{3h} in (b) are distorted to C_s and C_s, respectively.

Eu^{3+} is displaced as shown in the right of Figure 1a, the local site symmetry for the Eu^{3+} subset will be exactly C_s. For β-$NaYF_4$, as there is only one Y site observed (as will be revealed by our spectroscopic evidence later), it is reasonable to assume that the space group for β-$NaYF_4$ is $P6_3/m$, instead of $P\bar{6}$ with two kind of crystallographic sites for Y^{3+}. According to single-crystal XRD data, there are two types of cationic sites in a unit cell for the space group of $P6_3/m$: one nine-fold coordinated site occupied randomly by Na^+ and Y^{3+} (site 2c, symmetry of C_{3h}), which is coordinated by nine nearest-neighboring F^- ions in the shape of a tricapped trigonal prism and 2 Na^+ and 6 Y^{3+} in the second-nearest-neighboring shell,[1g] another six-fold coordinated site is occupied by Na^+ and vacancies (site 2b; Figure 1b, left). When Eu^{3+} ions are doped, for the same reason mentioned above for α-$NaYF_4$, the local site symmetry of all Eu^{3+} subsets will descend from C_{3h} to lower symmetries, such as C_s, C_3, or C_1, depending on the displacement pattern of Y/Na on site 2c in the second coordination shell around each subset of Eu. If Y/Na on site 2c around one subset of Eu^{3+} are displaced as shown in the right of Figure 1b, the local site symmetry for this subset of Eu^{3+} will be exactly C_s.

To probe the practical local structure around Ln^{3+} dopants in both α- and β-$NaYF_4$, we measured the high-resolution photoluminescence (PL) spectra of $NaYF_4$:Eu^{3+} samples. Emission and excitation spectra and PL decays were recorded at low temperature (10 K) to avoid the thermal broadening of spectral bands at room temperature.[12] Figure 2 shows the PL spectra of Eu^{3+} in β- and α-$NaYF_4$ at 10 K, which enables a detailed assignment of the CF transition lines of Eu^{3+}. Total numbers of 1, 3, and 5 CF transition lines from $^5D_0$ to $^7F_0$, $^7F_1$, and $^7F_2$ were observed in the emission spectrum of β-$NaYF_4$:Eu^{3+} upon excitation at 393 nm (Figure 2a), indicating a complete lifting of degeneracy of ^7F_J at a rather low site symmetry. To make sure whether all these lines arose from the

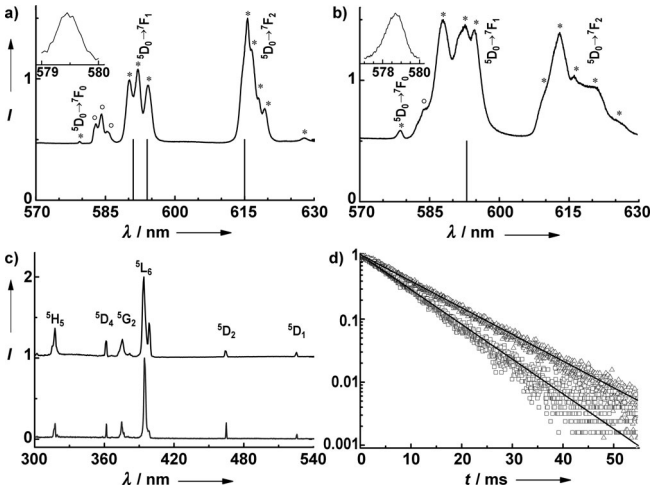

Figure 2. a) 10 K PL emission spectra of Eu^{3+} in β-$NaYF_4$ (upper) and theoretically allowed transition lines at a C_{3h} site (lower). b) 10 K PL emission spectra of Eu^{3+} in α-$NaYF_4$ (upper) and theoretically allowed transition lines at an O_h site (lower). In (a) and (b), the inset shows an enlargement of the $^5D_0 \rightarrow {}^7F_0$ transition; the crystal-field transition lines from $^5D_0$ to $^7F_0$, $^7F_1$ and $^7F_2$ are marked by asterisks, and the emission peaks at about 585 nm owing to the $^5D_1 \rightarrow {}^7F_3$ transition are marked by circles. c) 10 K PL excitation spectra (upper: α-$NaYF_4$:Eu^{3+}, lower: β-$NaYF_4$:Eu^{3+}) and d) decay curves of Eu^{3+} in α- (△) and β-$NaYF_4$:Eu^{3+} crystals (□) by monitoring the characteristic emission of $^5D_0 \rightarrow {}^7F_1$ of Eu^{3+}. Line in (d): fit to the data.

same site, site-selective excitation spectra were measured by monitoring the three peaks of $^5D_0 \rightarrow {}^7F_1$ at 594.3, 592.1, and 590.2 nm. All of these excitation spectra are coincident (Supporting Information, Figure S3), which indicates that the luminescence originated from Eu^{3+} occupying the same kind of spectroscopic site, and verifies that the space group for β-$NaYF_4$ rods could be $P6_3/m$. In this structure model, Eu^{3+} ions replacing Y^{3+} should be ideally located at a crystallographic site with symmetry of C_{3h} in theory. If the doped Eu^{3+} ions remained with such a C_{3h} symmetry, the $^5D_0 \rightarrow {}^7F_0$ emissions would be strictly forbidden, and the number of $^5D_0 \rightarrow {}^7F_{1,2}$ emission lines would be 2 and 1, respectively (Figure 2a, lower).[13] However, the appearance of the $^5D_0 \rightarrow {}^7F_0$ transition in Figure 2a infers that the site symmetry of Eu^{3+} in β-$NaYF_4$ should be restricted to C_s, C_n, or C_{nv} ($n = 1, 2, 3, 4, 6$). According to the branching rules (Supporting Information, Figure S4) and transition selection rules of the 32 point groups (Supporting Information, Table S2),[14] the highest site symmetry of Eu^{3+}, distorted from C_{3h}, is deduced to be C_s based on the above spectroscopic evidence.

Similarly, for α-$NaYF_4$, Eu^{3+} ions substituting Y^{3+} ions would ideally possess a crystallographic site with point-group symmetry of O_h. In principle, the $^5D_0 \rightarrow {}^7F_{0,2,4}$ emissions that are of forced electric-dipole nature should be strictly forbidden, and only the magnetic-dipole transition of $^5D_0 \rightarrow {}^7F_1$ would be allowed and thus be observed in the PL spectrum of Eu^{3+} (Figure 2b, lower).[13] However, the integrated PL intensity of the $^5D_0 \rightarrow {}^7F_2$ transition was found comparable to that of $^5D_0 \rightarrow {}^7F_1$, which unambiguously supports that local Eu^{3+} ions occupy a much lower site symmetry than O_h. The numbers of CF transition lines from $^5D_0$ to $^7F_0$, $^7F_1$, and $^7F_2$ are 1, 3, and 5, respectively (Figure 2b). Therefore, the highest site symmetry of Eu^{3+}, distorted from O_h, should be C_s or C_2, according to the branching rules and transition selection rules of the 32 point groups. Breakdown of crystallographic site symmetry from O_h to C_s or C_2 was also observed in cubic $KLaF_4$ and $KGdF_4$ nanocrystals with the same crystal structure (Supporting Information, Figure S5).

The PL decays were measured by monitoring the characteristic emission of Eu^{3+} (Figure 2d). Both PL decay profiles show single exponential form, and the PL lifetimes of $^5D_0$ were determined to be 10.27 and 7.78 ms at 10 K for Eu^{3+} in α- and β-$NaYF_4$, respectively. Such single-exponential decay behavior also indicates the nearly homogeneous CF environment around Ln^{3+} in the single lattice sites.[15] The observed PL lifetime of the excited states of Eu^{3+} is the reciprocal of the total transition rate that consists of both nonradiative and radiative transition rates.[3e] The nonradiative part depends basically on the maximum phonon energy of the host, while the radiative part is sensitive to the local site symmetry owing to forced electric-dipole transitions in noncentrosymmetric site.[3b–e] By using the integrated PL intensity of $^5D_0 \rightarrow {}^7F_1$ as the internal reference,[3b] the radiative lifetimes of $^5D_0$ were calculated to be 11.31 and 6.57 ms from the emission spectra of α- and β-$NaYF_4$, respectively, which are consistent with their observed values. This further confirms that the decay of $^5D_0$ occurs mainly by a radiative process. In this sense, the PL lifetime of $^5D_0$ also depends on the structural information such as distortion of ligand environment and site symmetry. The theoretical radiative lifetime of $^5D_0$ would be 22.39 ms and much longer than the observed if we assumed Eu^{3+} in α-$NaYF_4$ with exact crystallographic site symmetry of O_h in which only the magnetic-dipole transition of $^5D_0 \rightarrow {}^7F_1$ is allowed. Likewise, for Eu^{3+} ions in Cs_2NaYF_6 with site symmetry of O_h, the PL lifetime of $^5D_0$ was observed to be 15.0 ms,[3f] which is markedly longer than that of Eu^{3+} in α-$NaYF_4$. These site-symmetry-dependent decay behaviors further show that Eu^{3+} ions in α-$NaYF_4$ occupy a site with lower symmetry than crystallographic site symmetry of O_h.

The breakdown from crystallographic site symmetry will significantly affect the spectral line-width of Ln^{3+}. A typical optical spectrum of Eu^{3+} in ordered crystals (such as In_2O_3 and Gd_2O_3) usually exhibits remarkably sharp and well-resolved peaks with a full-width at half-maximum (FWHM) typically in the range of 0.1–0.5 nm, which is consistent with the fact that Eu^{3+} ions occupy well-defined locations in the lattice.[16] By contrast, owing to the minute structural distortion mentioned above, a locally variable CF surrounding around the dopant will happen in disordered crystals, which imposes a slightly different CF on each subset of Eu^{3+} ions. An average CF environment for whole set of Eu^{3+} ions is often experimentally defined because of the indiscernibility of the Eu subsets, even with the aid of state-of-the-art spectroscopic equipments. As a consequence, the linewidths of the electronic transitions for Ln^{3+} are usually inhomogeneously broadened relative to that in ordered crystals.[5,17] As shown in Figure 2a,b, the emission lines are broad for Eu^{3+} in α- and β-$NaYF_4$ phosphors even at 10 K, with average FWHMs of 3.2 and 1.8 nm, respectively. amplified the emission peak of the $^5D_0 \rightarrow {}^7F_0$ transition in α-$NaYF_4$:Eu^{3+} in Figure 3. The

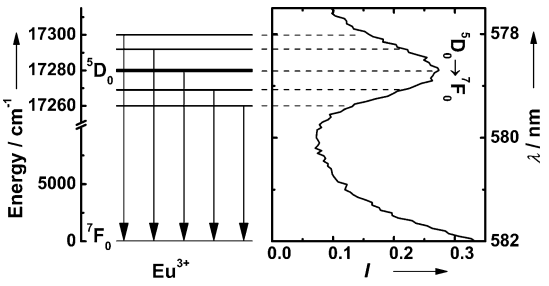

Figure 3. Illustration showing an overall inhomogeneous line broadening of the $^5D_0 \rightarrow {}^7F_0$ transition owing to spectral superimposition from different subsets of Eu^{3+} ions in α-$NaYF_4$ as a result of crystallographic site-symmetry breakdown.

typical FWHM of this 0–0 transition line is about 0.1 nm in ordered crystals;[16a] however, it is markedly broadened to about 1.3 nm in α-$NaYF_4$. Such a line broadening is illustrated by the energy level diagram in Figure 3: in α-$NaYF_4$:Eu^{3+}, the second-nearest-neighboring ions around Eu^{3+}, 6 Na^+ and 6 Y^{3+}, are randomly distributed over the same lattice site 4a (Figure 1 a), which could exert slightly different CF on each subset of Eu^{3+} dopants. Accordingly, the exact energy level position of $^5D_0$ relative to $^7F_0$ differs slightly for each subset of Eu^{3+} ion with different CF surroundings. Such a level broadening will eventually lead to the closely lying emission lines of $^5D_0 \rightarrow {}^7F_0$ at slightly different transition wavelengths; that is, an overall inhomogeneous line broadening of the 0–0 transition.

To further verify the spectroscopic site symmetry of Eu^{3+} in α- and β-$NaYF_4$, energy level fitting of Eu^{3+} was carried out based on meticulous energy level assignments from the excitation and emission spectra at 10–300 K. A total of 48 and 58 CF levels of Eu^{3+} in α- and β-$NaYF_4$ were identified, respectively, which span an energy range of 0–36 000 cm^{-1} and belong to 38 multiplets of the $4f^6$ configuration of Eu^{3+} (Supporting Information, Tables S3, S4). The energy level fitting was performed by assuming the site symmetry of C_s for both α- and β-$NaYF_4$, using f-shell empirical programs.[18] The free-ion (FI) parameters of LaF_3:Eu^{3+} [19] and CF parameters of Gd_2O_3:Eu^{3+} [16a] were used as starting values for fitting. All of the independent CF parameters except B_0^k are complex with real and imaginary parts denoted by $\mathrm{Re}B_q^k$ and $\mathrm{Im}B_q^k$, because of the low site symmetry of Eu^{3+}. By means of the parametrization of an effective operator Hamiltonian including freely varied 16 FI and 14 CF parameters, energy-level fitting yielded root-mean-square deviations of 13.5 and 13.8 cm^{-1} for α- and β-$NaYF_4$, respectively. The CF strength of Eu^{3+} ions in α- and β-$NaYF_4$ was calculated to be 566 and 385 cm^{-1}, respectively, according to Chang's definition.[20] Usually a lower site symmetry occupied by Ln^{3+} ions in the host will result in a larger CF strength.[16] The observed CF strength of Eu^{3+} in $NaYF_4$ is relatively large as compared to those halide crystals reported with higher site symmetries of Eu^{3+} (Supporting Information, Table S5),[16a] which justifies the low site symmetry of Eu^{3+} in α- and β-$NaYF_4$. The optimal FI and CF parameters in the final fit were listed in the Table 1 and the Supporting Information, Table S6, and the fitted energy levels were compared with experimental values

Table 1: CF parameters of Eu^{3+} in α- and β-$NaYF_4$ crystals [cm^{-1}].[a]

Parameter	α-$NaYF_4$	β-$NaYF_4$	Parameter	α-$NaYF_4$	β-$NaYF_4$
B_0^2	271(46)	160(43)	B_0^6	564(93)	730(108)
B_2^2	321(26)	−347(24)	$\mathrm{Re}B_2^6$	512(71)	−47(119)
B_0^4	406(63)	−415(65)	$\mathrm{Im}B_2^6$	−208(129)	432(77)
$\mathrm{Re}B_2^4$	−27(85)	304(60)	$\mathrm{Re}B_4^6$	110(88)	−65(121)
$\mathrm{Im}B_2^4$	394(72)	415(61)	$\mathrm{Im}B_4^6$	179(135)	393(89)
$\mathrm{Re}B_4^4$	1441(83)	132(99)	$\mathrm{Re}B_6^6$	989(350)	−304(441)
$\mathrm{Im}B_4^4$	−237(302)	248(70)	$\mathrm{Im}B_6^6$	−988(274)	1104(128)

[a] Values in parentheses are errors in the indicated parameters that were freely varied in the fit.

(Supporting Information, Tables S3 and S4). Most fitted energy levels of Eu^{3+} in α- and β-$NaYF_4$ shift within a range from 0 to 30 cm^{-1}. Such small standard deviations show a very satisfying agreement between the calculated and observed levels, which thus verify the rationality of the C_S symmetry assignment of Eu^{3+} and directly supports the breakdown of crystallographic site symmetry in α- and β-$NaYF_4$:Eu^{3+} phosphors. Both sets of reliable CF parameters are determined for the first time, which can be used as an important reference to deduce CF and local structures of other Ln^{3+} ions in $NaYF_4$ phosphors.

To ascertain whether the spectroscopic site symmetry changes with the dopant concentration, α- and β-$NaYF_4$ samples doped with various concentration of Eu^{3+} (0.5, 5, and 20 mol%) were synthesized. The line positions in RT emission and excitation spectra of all of the samples are identical and independent of the Eu^{3+} concentration, which consist of the fingerprint peaks originating from the same Eu^{3+} site (Figure 4; Supporting Information, Figure S6). This observation clearly demonstrates that the spectroscopic site symmetry of Eu^{3+} does not change with the dopant concen-

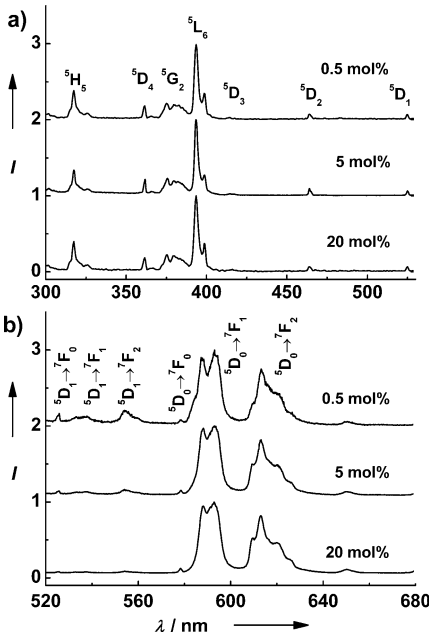

Figure 4. a) Excitation and b) emission spectra of α-$NaYF_4$:Eu^{3+} crystals (0.5, 5, and 20 mol%) at RT.

tration in either α- or β-$NaYF_4$, in view of their unaltered CF splittings. Note that the intensity ratio of the $^5D_1 \rightarrow {}^7F_J$ ($J = 0,1,2,3,4$) to that of $^5D_0 \rightarrow {}^7F_J$ ($J = 0,1,2,3,4$) decreases markedly with the Eu^{3+} concentration in the RT emission spectra (Figure 4). This phenomenon is caused by the cross relaxations between adjacent Eu^{3+} ions that depend critically on the distance between two Eu^{3+} emitters.[21] The $^5D_0 \rightarrow {}^7F_0$ transition at 578.6 nm appears even at RT, indicating an acentric site symmetry of Eu^{3+} in all cubic samples,[22] which is consistent with the observations at 10 K.

The effect of the Eu^{3+} concentration on the PL lifetime of $^5D_0$ of Eu^{3+} in β-$NaYF_4$ was further studied by monitoring the dominant emission of Eu^{3+} (Supporting Information, Figure S7). The PL decays from $^5D_0$ of Eu^{3+} at low concentrations (0.5 and 5 mol%) show a noticeable rising edge at the initial stage and a single-exponential decay in the tail when excited to the higher energy level ($^5L_6$). The rise times for these two samples were determined to be 2.58 and 1.13 ms, respectively, by fitting the rising edge of the decay curves (Supporting Information, Figure S7, inset). Furthermore, the PL lifetimes of $^5D_1$ for these two samples were measured to be 3.27 and 1.51 ms (Supporting Information, Figure S8), respectively, which essentially agree well with those of the rise times. These results reveal that the population of $^5D_0$ was most likely due to the nonradiative relaxation from $^5D_1$ and higher excited states. As such, the rise time will decrease with increasing Eu^{3+} concentration owing to enhanced cross relaxations between adjacent Eu^{3+} ions. In fact, no rising edge was observed in the PL decay of $^5D_0$ at the Eu^{3+} concentration of 20 mol%. The intrinsic PL lifetime of $^5D_0$ level can be determined to be 7.98, 7.32, and 6.96 ms from the tail of corresponding decays with increasing Eu^{3+} concentration (0.5, 5, and 20 mol%). The single-exponential decays at various Eu^{3+} concentrations confirm the existence of only single spectroscopic site of Eu^{3+}. The slightly shorter PL lifetime of Eu^{3+} observed at RT is attributed to an increase in nonradiative transition rate with the temperature that leads to an increase in total transition rate.[23]

In summary, single-crystal XRD indicates that Y^{3+} ions are located at the high-symmetry crystallographic site in disordered α- and β-$NaYF_4$ crystals, and it is often assumed that the doped Eu^{3+} ions occupy the site of Y^{3+} with identical crystallographic point group symmetry because of their same charge and similar ionic radii. However, high-resolution PL spectroscopy by employing Eu^{3+} as the structural probe has revealed that the highest spectroscopic site symmetries of Eu^{3+} descend from crystallographic O_h to C_s (or C_2) in α-$NaYF_4$, and from crystallographic C_{3h} to C_s in β-$NaYF_4$, respectively. The breakdown of crystallographic site symmetry in such disordered crystals, independent of the dopant concentration, has been further confirmed by the crystal-field level fitting, which yielded a very small standard deviation from the experiments. The spectral linewidth of emitters in disordered sites is broadened owing to spectral superimposition from different subsets of dopants. A similar breakdown of crystallographic site symmetry can be observed in other disordered crystals, such as cubic $KLaF_4$ and $KGdF_4$. A comprehensive understanding the photoactive site symmetry breakdown and the actual CF around lanthanides in this huge family of crystals is of vital importance for their further applications in the fields of luminescent bioassays, lighting, and displays.

Received: October 12, 2012
Revised: November 6, 2012
Published online: December 6, 2012

Keywords: lanthanides · $NaYF_4$ · photoluminescence · structure elucidation · symmetry

[1] a) F. Auzel, *Chem. Rev.* **2004**, *104*, 139–173; b) G. F. Wang, Q. Peng, Y. D. Li, *Acc. Chem. Res.* **2011**, *44*, 322–332; c) H. X. Mai, Y. W. Zhang, R. Si, Z. G. Yan, L. D. Sun, L. P. You, C. H. Yan, *J. Am. Chem. Soc.* **2006**, *128*, 6426–6436; d) J. W. Wang, J. H. Hao, P. A. Tanner, *Opt. Express* **2011**, *19*, 11753–11758; e) M. Haase, H. Schäfer, *Angew. Chem.* **2011**, *123*, 5928–5950; *Angew. Chem. Int. Ed.* **2011**, *50*, 5808–5829; f) C. C. Lin, Z. R. Xiao, G. Y. Guo, T. S. Chan, R. S. Liu, *J. Am. Chem. Soc.* **2010**, *132*, 3020–3028; g) F. Wang, Y. Han, C. S. Lim, Y. H. Lu, J. Wang, J. Xu, H. Y. Chen, C. Zhang, M. H. Hong, X. G. Liu, *Nature* **2010**, *463*, 1061–1065.

[2] a) S. W. Hao, L. Sun, G. Y. Chen, H. L. Qiu, C. Xu, T. N. Soitah, Y. Sun, C. H. Yang, *J. Alloys Compd.* **2012**, *522*, 74–77; b) O. Lehmann, K. Kömpe, M. Haase, *J. Am. Chem. Soc.* **2004**, *126*, 14935–14942.

[3] a) Y. H. Wang, Y. S. Liu, Q. B. Xiao, H. M. Zhu, R. F. Li, X. Y. Chen, *Nanoscale* **2011**, *3*, 3164–3169; b) M. H. V. Werts, R. T. F. Jukes, J. W. Verhoeven, *Phys. Chem. Chem. Phys.* **2002**, *4*, 1542–1548; c) A. M. Cross, P. S. May, F. C. J. M. van Veggel, M. T. Berry, *J. Phys. Chem. C* **2010**, *114*, 14740–14747; d) J. C. Boyer, F. Vetrone, J. A. Capobianco, A. Speghini, M. Bettinelli, *J. Phys. Chem. B* **2004**, *108*, 20137–20143; e) A. Kar, A. Patra, *Nanoscale* **2012**, *4*, 3608–3619; f) P. A. Tanner, Y. L. Liu, N. M. Edelstein, K. M. Murdoch, N. M. Khaidukov, *J. Phys. Condens. Matter* **1997**, *9*, 7817–7836.

[4] a) C. D. Donegá, S. Schenker, H. F. Folkerts, A. Meijerink, G. Blasse, *J. Phys. Condens. Matter* **1994**, *6*, 6043–6056; b) M. Rico, J. Liu, U. Griebner, V. Petrov, M. D. Serrano, F. Esteban-Betagon, C. Cascales, C. Zaldo, *Opt. Express* **2004**, *12*, 5362–5367.

[5] A. Aebischer, M. Hostettler, J. Hauser, K. Krämer, T. Weber, H. U. Güdel, H. B. Bürgi, *Angew. Chem.* **2006**, *118*, 2869–2873; *Angew. Chem. Int. Ed.* **2006**, *45*, 2802–2806.

[6] a) D. Yang, G. Li, X. Kang, Z. Cheng, P. Ma, C. Peng, H. Lian, C. Li, J. Lin, *Nanoscale* **2012**, *4*, 3450–3459; b) Y. J. Sun, Y. Chen, L. J. Tian, Y. Yu, X. G. Kong, J. W. Zhao, H. Zhang, *Nanotechnology* **2007**, *18*, 275609; c) L. Y. Wang, Y. D. Li, *Chem. Mater.* **2007**, *19*, 727–734; d) G. Y. Chen, T. Y. Ohulchanskyy, S. Liu, W. C. Law, F. Wu, M. T. Swihart, H. Ågren, P. N. Prasad, *ACS Nano* **2012**, *6*, 2969–2977; e) A. Xia, M. Chen, Y. Gao, D. Wu, W. Feng, F. Li, *Biomaterials* **2012**, *33*, 5394–5405; f) J. C. Zhou, Z. L. Yang, W. Dong, R. J. Tang, L. D. Sun, C. H. Yan, *Biomaterials* **2011**, *32*, 9059–9067.

[7] a) G. C. Jiang, J. Pichaandi, N. J. J. Johnson, R. D. Burke, F. C. J. M. van Veggel, *Langmuir* **2012**, *28*, 3239–3247; b) S. Mishra, G. Ledoux, E. Jeanneau, S. Daniele, M. F. Joubert, *Dalton Trans.* **2012**, *41*, 1490–1502; c) Y. Q. Sui, K. Tao, Q. Tian, K. Sun, *J. Phys. Chem. C* **2012**, *116*, 1732–1739.

[8] a) J. H. Burns, *Inorg. Chem.* **1965**, *4*, 881–886; b) K. W. Krämer, D. Biner, G. Frei, H. U. Güdel, M. P. Hehlen, S. R. Lüthi, *Chem. Mater.* **2004**, *16*, 1244–1251; c) B. P. Sobolev, D. A. Mineev, V. P. Pashutin, *Dokl. Akad. Nauk SSSR* **1963**, *150*, 791–794; d) G. D. Brunton, H. Insley, T. N. McVay, R. E. Thoma, *Crystallographic data for some metal fluorides, chlorides, and oxides*, Oak Ridge

National Laboratory Report No. ORNL-3761, Oak Ridge, Tennessee, **1965**.

[9] a) X. Liang, X. Wang, J. Zhuang, Q. Peng, Y. D. Li, *Adv. Funct. Mater.* **2007**, *17*, 2757 – 2765; b) Z. L. Wang, J. H. Hao, H. L. W. Chan, W. T. Wong, K. L. Wong, *Small* **2012**, *8*, 1863 – 1868; c) P. Ghosh, A. Patra, *J. Phys. Chem. C* **2008**, *112*, 19283 – 19292; d) C. Renero-Lecuna, R. Martín-Rodríguez, R. Valiente, J. González, F. Rodríguez, K. W. Krämer, H. U. Güdel, *Chem. Mater.* **2011**, *23*, 3442 – 3448.

[10] A. Grzechnik, P. Bouvier, M. Mezouar, M. D. Mathews, A. K. Tyagi, J. Kohler, *J. Solid State Chem.* **2002**, *165*, 159 – 164.

[11] a) D. Zakaria, M. T. Fournier, R. Mahiou, J. C. Cousseins, *J. Alloys Compd.* **1992**, *188*, 250 – 254; b) N. Martin, P. Boutinaud, M. Malinowski, R. Mahiou, J. C. Cousseins, *J. Alloys Compd.* **1998**, *275*, 304 – 306.

[12] A. Bednarkiewicz, A. Mech, M. Karbowiak, W. Strek, *J. Lumin.* **2005**, *114*, 247 – 254.

[13] Q. Ju, D. T. Tu, Y. S. Liu, R. F. Li, H. M. Zhu, J. C. Chen, Z. Chen, M. D. Huang, X. Y. Chen, *J. Am. Chem. Soc.* **2012**, *134*, 1323 – 1330.

[14] a) Q. Ju, Y. S. Liu, R. F. Li, L. Q. Liu, W. Q. Luo, X. Y. Chen, *J. Phys. Chem. C* **2009**, *113*, 2309 – 2315; b) P. H. Butler, *Point Group Symmetry Application: Method and Tables*, Plenum, New York, **1981**.

[15] C. X. Li, Z. W. Quan, J. Yang, P. P. Yang, J. Lin, *Inorg. Chem.* **2007**, *46*, 6329 – 6337.

[16] a) L. Q. Liu, X. Y. Chen, *Nanotechnology* **2007**, *18*, 255704; b) Q. B. Xiao, Y. S. Liu, L. Q. Liu, R. F. Li, W. Q. Luo, X. Y. Chen, *J. Phys. Chem. C* **2010**, *114*, 9314 – 9321.

[17] G. Huber, W. Lenth, J. Lieberts, F. Lutz, *J. Lumin.* **1978**, *16*, 353 – 360.

[18] M. F. Reid, f-shell empirical programs and examples (personal communication).

[19] W. T. Carnall, G. L. Goodman, K. Rajnak, R. S. Rana, Argonne National Laboratory Report No. ANL-88 – 8, Argonne, Illinois, **1988**.

[20] N. C. Chang, J. B. Gruber, R. P. Leavitt, C. A. Morrison, *J. Chem. Phys.* **1982**, *76*, 3877.

[21] Y. S. Liu, D. T. Tu, H. M. Zhu, R. F. Li, W. Q. Luo, X. Y. Chen, *Adv. Mater.* **2010**, *22*, 3266 – 3271.

[22] P. Ptacek, H. Schäfer, K. Kömpe, M. Haase, *Adv. Funct. Mater.* **2007**, *17*, 3843 – 3848.

[23] H. W. Song, L. X. Yu, S. Z. Lu, T. Wang, Z. X. Liu, L. M. Yang, *Appl. Phys. Lett.* **2004**, *85*, 470 – 472.

